J. Fluid Mech. (2018), *vol.* 844, *pp.* 796–816. © Cambridge University Press 2018
doi:10.1017/jfm.2018.205

Mean shear versus orientation isotropy: effects on inertialess spheroids' rotation mode in wall turbulence

Kun Yang[1], Lihao Zhao[2,1,†] and Helge I. Andersson[1]

[1]Department of Energy and Process Engineering, Norwegian University of Science and Technology, 7491 Trondheim, Norway

[2]AML, Department of Engineering Mechanics, Tsinghua University, 10084 Beijing, China

(Received 7 September 2017; revised 13 February 2018; accepted 27 February 2018)

The orientation of spheroidal particles dispersed in a fluid flow is known to influence the particles' rotation mode. Rod-like and disk-like particles orient themselves differently and accordingly also rotate differently. In order to explore the role of the deterministic factors, i.e. mean shear and vorticity anisotropy, on the orientational behaviour of inertialess tracer spheroids, we adopted a purpose-made Couette–Poiseuille flow simulated numerically by Yang *et al.* (*Intl J. Heat Fluid Flow*, vol. 63, 2017, pp. 14–27). Typical wall turbulence with streamwise-oriented streaky structures caused by the locally high mean shear rate was observed only at one of the walls. The absence of mean shear at the other wall gave rise to an atypical turbulence field. Over a relatively wide and quasi-homogeneous core region, a modest mean shear rate made the vorticity field anisotropic. In spite of the mean shear, rod-like tracers were spinning and disk-like spheroids were tumbling, just as in homogeneous isotropic turbulence. We explained this phenomenon by the isotropic particle orientation and concluded that zero mean shear is not necessary for rod spinning and disk tumbling. The orientation and rotation of the Lagrangian tracer spheroids near the high shear wall were almost indistinguishable from the well-known behaviour in turbulent channel flows. Near the opposite wall, where the mean shear was negligibly small, disk-like particles aligned preferentially in the wall-normal direction and rotated similarly as in the presence of high shear. Rod-like particles, on the contrary, aligned more randomly and accordingly rotated similarly as in the core region. These observations revealed that the degree of particle orientation anisotropy has a major impact on the particle rotation mode, whereas mean shear, irrespective of the actual shear rate, only plays a secondary role in particle rotation. Deduction of the eigenvectors of the left Cauchy–Green tensor showed that the preferential orientation of the tracer spheroids was caused by the alignment of rods and disks with the strongest Lagrangian stretching and compression directions, respectively. Lagrangian stretching/compression determines the particle orientations and the particle orientation affects the particle rotation mode.

Key words: multiphase and particle-laden flows, particle/fluid flow

† Email address for correspondence: zhaolihao@tsinghua.edu.cn

1. Introduction

Tiny particles with non-spherical shape are encountered in a variety of natural and industrial processes (Voth & Soldati 2017). A prominent example is plankton in oceanic flows (Pedley & Kessler 1992; Guasto, Rusconi & Stocker 2012). The various shapes of plankton have probably evolved through natural selection since shape is likely to affect their ability to feed and reproduce. Turbulence (Ruiz, Macías & Peters 2004; Barry *et al.* 2015) and shape (Siewert *et al.* 2014) are known to affect the sinking rate of plankton-like particles and their eventual deposition in homogeneous isotropic turbulence (HIT). The hydrodynamic forces depend on the plankton-particle alignment with the flow, which is altered by the presence of mean shear (Reidenbach, Koseff & Koehl 2009). Recently, Ardeshiri *et al.* (2016, 2017) demonstrated the crucial role of local shear in copepods' dynamics. The ability of copepods to escape from localized high strain rates affects their preferential concentration and thereby also the growth and reproduction rates.

1.1. *Dynamics of tracer non-spherical particles*

Inertia-free particles passively follow the translational fluid motion irrespective of their shape, whereas only spherical tracer particles rotate along with the fluid vorticity. Although non-spherical particles are oriented randomly with respect to an inertial reference frame in HIT, their anisotropic shape induces a preferential alignment with the local velocity gradient tensor (Pumir & Wilkinson 2011). Computational studies showed that rod-like particles tend to align their symmetry axis $\boldsymbol{p}$ with the instantaneous vorticity vector $\boldsymbol{\Omega}$ (Parsa *et al.* 2012, Byron *et al.* 2015), whereas disk-like particles preferentially orient $\boldsymbol{p}$ perpendicular to $\boldsymbol{\Omega}$ (Gustavsson, Einarsson & Mehlig 2014; Byron *et al.* 2015). The qualitatively different alignments of rod- and disk-like particles impact on their rotational behaviours such that the rods spin and disks tumble. These findings are supported by sophisticated laboratory measurements by Parsa *et al.* (2012), Marcus *et al.* (2014) and Ni *et al.* (2015). They used multiple cameras with viewing axes in different planes to allow the full fibre orientation vector $\boldsymbol{p}$ to be determined. In spite of the shape dependence of the partition between spinning and tumbling rates of non-spherical particles, the full solid-body rotation rate is nevertheless almost independent of the actual particle shape; see e.g. Parsa *et al.* (2012) and Byron *et al.* (2015).

The orientation and rotation of non-spherical tracer particles have also been studied in turbulent channel flows which serve as a prototype of wall-bounded turbulence (WT). Although particles orient almost randomly in the centre of the channel, where the vorticity field is nearly isotropic (Andersson, Zhao & Variano 2015), the alignment near the channel walls depends crucially on aspect ratio. Disk-like particles strongly align their symmetry axis $\boldsymbol{p}$ in the wall-normal direction, whereas rod-like tracer particles align parallel with the wall and mostly in the streamwise direction (Challabotla, Zhao & Andersson 2015*b*). The strong preferential orientation of non-spherical particles reduces the mean particle rotation $\langle\omega\rangle$ below that for spheres, the latter of which equals the mean fluid rotation $\langle\Omega\rangle$. In spite of the substantial reduction of mean angular velocity $\langle\omega\rangle$ of tracers with high asphericity, enhanced fluctuations of the streamwise component of the angular velocity were observed by Challabotla *et al.* (2015*b*).

Zhao *et al.* (2015) showed that there are two qualitatively different rotation modes of tracer spheroids in channel-flow turbulence. Just as in HIT (Parsa *et al.* 2012; Byron *et al.* 2015), rods preferentially spin and disks tumble in the central region (Mode I). In the near-wall region, however, both tumbling and spinning are suppressed with increasing asphericity (Mode II). Spheroidal particles in Mode I are nearly

randomly oriented in the channel centre, where the mean shear vanishes and the vorticity field is almost isotropic. The local fluid vorticity vector $\boldsymbol{\Omega}$ and the orientation vector of rod-like particles $\boldsymbol{p}$ are both preferentially aligned in the strongest Lagrangian stretching direction, while disk-like particles orient in the Lagrangian compression direction, which is perpendicular to the fluid vorticity vector (Ni, Ouellette & Voth 2014; Zhao & Andersson 2016). The shape-dependent particle rotational behaviour is therefore caused by how an aspherical particle orients itself relative to the local fluid vorticity. In Mode II, rod- and disk-like spheroidal particles are preferentially aligned in the streamwise (Lagrangian stretching) direction and the wall-normal (Lagrangian compression) direction, respectively. The rotational behaviour is strongly affected by the mean shear (i.e. anisotropic fluid vorticity), and is therefore qualitatively consistent with a spheroid's rotation in uniform shear flow following so-called Jeffery orbits (Challabotla *et al.* 2015*b*). This suggests a negligible influence of the turbulent vorticity fluctuations. Although tracer spheroids are preferentially oriented in the Lagrangian stretching or compression direction in shear-dominated regions, the vorticity vector is essentially uncorrelated with Lagrangian stretching (Zhao & Andersson 2016). Accordingly, we hypothesize that the particle's preferential orientation and the rate of fluid shear are the two factors that determine the rotational mode of spheroidal tracer particles.

1.2. *Point particles versus fully resolved particles*

Particulate additives to a homogeneous fluid can be treated as point particles provided that the size δ of the additives are smaller than the tiniest turbulent eddies, i.e. the Kolmogorov length scale η. This assumption can be justified for several different applications, including planktonic organisms in the ocean. While $\eta \sim 0.1$–10 mm in marine turbulence (Jiménez 1997), phytoplankton cells are typically of size $\delta \sim 1$–100 μm (Durham *et al.* 2013). In addition to the size constraint, $\delta/\eta \ll 1$, the particle Reynolds number Re_p has to be smaller than one. This implies that the flow in the immediate vicinity of a particle can be considered as Stokesian, which is required in order to derive exact analytical expressions for the viscous forces and torques acting on the particle. However, approximate formulae aimed to be valid also for $Re_p > 1$ were recently derived and employed by Ouchene *et al.* (2016) and Arcen *et al.* (2017). The advantages and shortcomings of the point-particle approach to simulate dispersed multiphase flows have been discussed in review articles by Balachandar (2009), Eaton (2009) and Balachandar & Eaton (2010).

For larger particles, i.e. when the particle size is larger than the Kolmogorov length, the point-particle approach can no longer be justified. In direct numerical simulation of particle-laden flows major difficulties arise with respect to the treatment of the solid surface of each of the moving particles. The particles occupy parts of the computational volume and the surface of the particle has to be embedded in the computational mesh. Four different approaches to numerically resolve the flow around each individual moving particle were summarized by Lucci, Ferrante & Elghobashi (2010). At that time these methods were only used to simulate finite-sized spherical particles in turbulence. More recently, however, Do-Quang *et al.* (2014), Rosén, Lundell & Aidun (2014) and Eshghinejadfard, Hosseini & Thevenin (2017) used a lattice-Boltzmann (LB) method, whereas Ardekani *et al.* (2017) used an immersed boundary (IB) method to simulate the motion of non-spherical particles in viscous fluid flow. Rosén *et al.* (2014) were concerned with the rotational dynamics of a single neutrally buoyant prolate spheroid in a laminar shear flow. Their fully resolved

LB simulation enabled an exploration of the competition between fluid inertia and particle inertia. Do-Quang *et al.* (2014) and Eshghinejadfard *et al.* (2017) also used a lattice-Boltzmann method to simulate the translational and rotational motion of elongated particles in turbulent channel flow. Do-Quang *et al.* (2014) considered cylindrical particles with aspect ratios from 2 to 15, whereas Eshghinejadfard *et al.* (2017) studied prolate spheroids with aspect ratios 1, 2 and 4. Ardekani *et al.* (2017), by means of an IB method, showed that finite-sized oblate spheroids with aspect ratio 1:3 could lead to drag reduction in turbulent channel flow. All these approaches to finite-sized particle simulations require additional computational efforts and the particle number in such simulations are therefore limited and typically of the order of 10 000.

1.3. *Wall turbulence in the absence of mean shear*

A characterizing feature of turbulent channel flows, i.e. pressure-driven plane Poiseuille flows, is the presence of near-wall streaks and coherent vortical structures educed by the locally high mean shear rate; see e.g. Kim, Moin & Moser (1987), Robinson (1991), Jeong *et al.* (1997). Strikingly similar near-wall turbulence is observed also in shear-driven plane Couette flow (Bech *et al.* 1995). Typical near-wall turbulence is accordingly associated with the presence of a relatively high mean shear rate at the solid wall. However, Lee, Kim & Moin (1990) demonstrated that elongated streaky flow structures developed also in the absence of a solid surface, provided that the mean shear rate was sufficiently high. On the other hand, Kuroda, Kasagi & Hirata (1995) showed that the streaky flow pattern along with the mean shear rate vanished near a moving wall in a Couette–Poiseuille flow, provided that the speed of the moving wall was adjusted with a view to eliminating the skin friction. Essentially the same flow field, but at higher Reynolds numbers, was examined independently by Coleman *et al.* (2017) and Yang, Zhao & Andersson (2017*b*).

Moving walls or belts are occasionally used in experimental facilities for a variety of different reasons. Practical occurrences of Couette–Poiseuille-type flows are beneath flat-bottomed vessels operating in shallow waters with small underkeel clearance (Gourlay 2006) and in the ground gap underneath a moving vehicle (Katz 2006). The turbulent Couette–Poiseuille flow has also been used by Thurlow & Klewicki (2000) and Spencer *et al.* (2009) to explore the mechanisms of drag reduction of ultrahydrophobic surfaces.

1.4. *Present study*

Despite the recent advances in the development of a phenomenology of preferential alignment and rotation in HIT and WT, as outlined in § 1.1, the actual role of mean shear has not yet been clarified and the following questions remain unanswered: What is the role played by mean shear in particle rotation in a turbulent flow? Do non-spherical particles exhibit preferential orientations in the absence of mean shear? Is the particle rotation mode, i.e., Mode I or Mode II, uniquely decided by the anisotropy of the particle orientation? To address these issues, the alignment and rotation of inertia-free spheroids with different shapes (from oblate to prolate) will be explored in a tailor-made Couette–Poiseuille flow (see § 2.1). The choice of spheroids without inertia frees the discussion of preferential concentration or turbophoresis. The numerically simulated flow field is designed with the view to have conventionally sheared wall turbulence at the stationary surface and shear-free conditions at the moving surface (Yang *et al.* 2017*b*). As an outcome, a wide core region resembles

almost homogeneous shear turbulence (HST); e.g. Sekimoto, Dong & Jiménez (2016). Our goal is to interpret the particles' rotation modes in the vicinity of the two differently sheared walls in terms of the spheroids' alignments with the fluid vorticity vector (§ 3.2) and with the Lagrangian stretching directions (§ 3.3).

2. Eulerian–Lagrangian modelling approach

2.1. *Turbulent Couette–Poiseuille flow with zero wall shear*

For the purpose of the present study, we realized a turbulent Couette–Poiseuille flow by means of direct numerical simulation (DNS). The flow between two parallel walls separated by a distance $2h$ was driven in the positive x-direction by means of a prescribed mean pressure gradient $\mathrm{d}P/\mathrm{d}x < 0$. The wall at $z = 0$ was at rest whereas the other wall at $z = 2h$ was moving in the x-direction with a constant speed U_w. U_w was systematically adjusted until the mean shear rate $\mathrm{d}U/\mathrm{d}z$ almost vanished at the moving wall. Thus, in the absence of friction at the moving wall, the shear stress τ_w at the stationary wall alone balanced the pressure gradient such that $\tau_w = -2h\,\mathrm{d}P/\mathrm{d}x$. The governing Navier–Stokes equations were integrated in time by means of an explicit Adams–Bashforth scheme while subjected to the mass conservation constraint. A pseudo-spectral method was used in the two homogeneous directions (x, y) whereas second-order finite-difference discretization was used in the wall-normal (z) direction (Mortensen *et al.* 2008). No slip and impermeability conditions were imposed at both walls whereas periodicity was assumed in the homogeneous directions.

The Reynolds number Re_τ based on the friction velocity $u_\tau = (\tau_w/\rho)^{1/2}$ and the wall separation distance $2h$ was 180. The simulation was performed on a $36h \times 10h \times 2h$ computational domain; see Yang *et al.* (2017*b*). This particular Couette–Poiseuille flow exhibited a monotonically increasing mean velocity all the way from the stationary wall to the moving wall with $U(z = 2h) = U_w = 20u_\tau$. The flow field near the stationary wall closely resembled conventional wall turbulence typically found in plane channel flows. Next to the moving wall, however, the anisotropy of the turbulence was qualitatively different with almost isotropic two-componential velocity and vorticity fluctuations in homogeneous wall-parallel (x, y)-planes. In a wide quasi-homogeneous central region, the mean shear rate $\mathrm{d}U/\mathrm{d}z$ turned out to be almost constant and approximately 1.5 % of the wall value. Elongated streaky structures were observed near the stationary wall, similarly to plane Poiseuille flows (e.g. Kim *et al.* 1987) and plane Couette flow (e.g. Richter & Sullivan 2013), whereas contours of streamwise velocity fluctuations near the moving surface revealed significantly shorter but wider flow structures, as shown in figure 9 in Yang *et al.* (2017*b*).

Even in the absence of mean shear, the moving wall exerts distinct effects on the nearby flow field due to pressure reflections from the wall and viscous damping of velocity fluctuations. The fluctuating velocity field approaches a two-dimensional (2-D) limit at the wall due to the impermeability condition which blocks wall-normal fluctuations. Similarly, the fluctuating vorticity field also approaches a 2-D limit in which the wall-normal vorticity is suppressed due to the no-slip conditions on the velocity components aligned with the shear-free wall (Yang *et al.* 2017*b*). These features make the turbulence in the vicinity of the moving wall distinctly different from the turbulent velocity and vorticity fluctuations near a free surface; see e.g. Handler *et al.* (1993), Pan & Banerjee (1995) and Nagaosa & Handler (2003).

The mean shear rate $\mathrm{d}U/\mathrm{d}z$ decreases almost monotonically with z from a high value at the stationary wall to almost zero at the moving wall. The reciprocal $(\mathrm{d}U/\mathrm{d}z)^{-1}$ can be considered as a characteristic time scale of the mean motion.

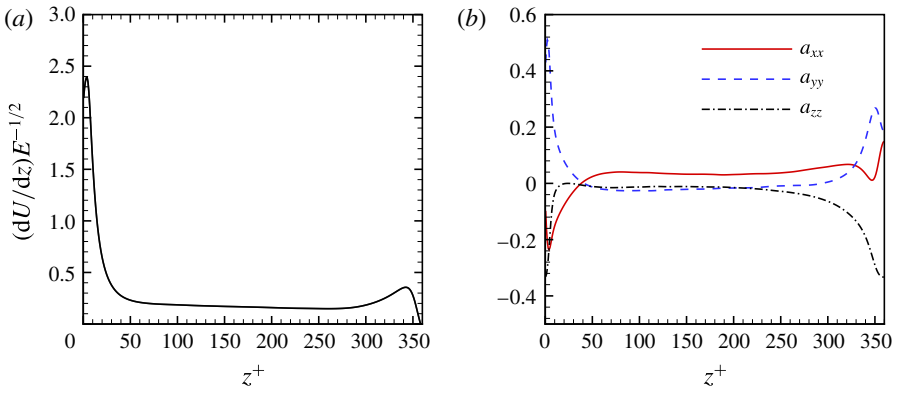

FIGURE 1. (Colour online) (*a*) The ratio between the mean vorticity to the square root of the enstrophy $(\mathrm{d}U/\mathrm{d}z)E^{-1/2}$; (*b*) the anisotropies of the vorticity fluctuations.

An often used turbulent time scale is k/ϵ. The ratio between the two time scales becomes $(k/\epsilon)/(\mathrm{d}U/\mathrm{d}z)^{-1} = (\mathrm{d}U/\mathrm{d}z)/(\epsilon/k)$. This is the dimensionless ratio used by Lee *et al.* (1990) in their study of strongly sheared homogeneous turbulence. They reported that streaky structures, like those found in near-wall turbulence, formed when the dimensionless shear rate parameter exceeded approximately 30. We can alternatively use the time scale $E^{-1/2}$ as representative of the turbulent vorticity where E is the enstrophy. The time scale ratio then becomes $E^{-1/2}/(\mathrm{d}U/\mathrm{d}z)^{-1} = (\mathrm{d}U/\mathrm{d}z)/E^{1/2}$. This is probably more relevant in the present context since we aim to compare the role of mean shear (or mean rotation) with the role of vorticity fluctuations in the spheroids' preferential orientations. The former time scale k/ϵ is representative of the energy-containing large-eddy motions whereas the latter time scale $E^{-1/2}$ characterizes the dissipative small-scale eddies.

Statistics and structures of the simulated Couette–Poiseuille flow were presented by Yang *et al.* (2017*b*). Since the vorticity field is believed to have a decisive impact on the rotation mode of the tracer spheroids, some results deduced from the flow simulation by Yang *et al.* (2017*b*) are shown in figure 1. The ratio between the mean vorticity to the square root of the enstrophy is provided in figure 1(*a*). The mean vorticity is by definition equal to two times the mean fluid rotation, i.e. $2\langle\Omega_y\rangle$, which in the present case happens to be equal to the mean shear rate $\mathrm{d}\langle U\rangle/\mathrm{d}z$. The enstrophy E is defined here as the trace of the second-moment tensor of the vorticity fluctuations $2\Omega_i'$, where the primes indicate deviations from the mean vorticity component $\langle 2\Omega_i\rangle$. The mean shear rate, and thus the mean vorticity, attains its highest value at the stationary wall from where it decreases monotonically almost all the way to the moving wall. The mean vorticity exceeds $E^{1/2}$ in the viscous-affected layer near the stationary wall. Over most of the cross-section, from $z^+ = 50$ to 300, the enstrophy measure $E^{1/2}$ is five times larger than the mean vorticity. It is particularly noteworthy that $\langle 2\Omega_y\rangle/E^{1/2}$ tends to zero at the moving wall, in contrast to behaviour near the stationary wall.

The anisotropies of the vorticity fluctuations are shown in figure 1(*b*). Here, the anisotropy of the streamwise vorticity fluctuations $\langle 2\Omega_x'\rangle$ is measured as:

$$a_{xx} = \frac{\langle 2\Omega_x' 2\Omega_x'\rangle}{\langle 2\Omega_i' 2\Omega_i'\rangle} - \frac{1}{3} = \frac{\langle \Omega_x' \Omega_x'\rangle}{\langle \Omega_i' \Omega_i'\rangle} - \frac{1}{3} \tag{2.1}$$

and similarly for a_{yy} and a_{zz} in the two other directions. We readily observe that a_{xx} is almost constant over a wide central region. That $a_{xx} > 0$ implies that the streamwise component of the vorticity fluctuations is larger than the fluctuations of the two other components of the vorticity vector. Although $a_{zz} \approx -1/3$ at both walls, as a direct consequence of the no-slip wall conditions, the vorticity fluctuation vector is oriented completely differently at the two walls. Fluctuations in the spanwise direction are totally dominating near the stationary wall, whereas streamwise fluctuations are equally important as spanwise vorticity fluctuations near the moving wall.

2.2. *Prolate spheroids as model of non-spherical tracers*

Solid particles are usually identified by a characteristic time scale τ_p which is a measure of how promptly a particle responds to changes in the local flow field. This relaxation time can be expressed as $\tau_p = 2\rho_p a^2 \Psi(\lambda)/9\mu = 2\rho_p a^2 \Psi(\lambda)/9\rho_f \nu$, where the shape function $\Psi(\lambda)$ can be expressed analytically for either oblate or prolate spheroids and becomes equal to 1.0 for spherical particles ($\lambda = 1$). If the particle relaxation time τ_p is much shorter than the shortest time scale of the turbulence, i.e. the Kolmogorov time scale τ_K, the particle responds almost immediately to turbulent fluctuations. Such particles are often referred to as tracers since they passively translate along with the flow. This limiting case when $\tau_p \ll \tau_K$ corresponds to a Stokes number $St = \tau_p/\tau_K \ll 1$. Such particles are also referred to as inertia free or non-inertial, which hints at the negligible influence of their inertia and does not necessarily imply that the particles are massless ($\rho_p = 0$). For instance in the case of neutrally buoyant spheres ($\rho_p = \rho_f$), $St \ll 1$ provided that the particle time scale $2a^2/9\nu$ is much smaller than the Kolmogorov time.

Such inertia-free particles travel with the same velocity as the local fluid and are unaffected by inertial drag and lift forces, both of which are related to the relative velocity between the particle and the fluid. Also the torques exerted by the viscous fluid on the spheroids become negligible in the $St \ll 1$ limit. Non-spherical particles will nevertheless rotate differently from the surrounding fluid. This phenomenon, which is in the focus of the present study, exists only for non-spherical particles with aspect ratios $\lambda \neq 1$.

Non-inertial spheroidal particles with aspect ratio λ (λ defined as the ratio between the symmetry axis and the two equal axes) were added into a turbulent channel-flow field and tracked by a Lagrangian approach (Challabotla *et al.* 2015*b*; Zhao & Andersson 2016). The tracer particles translate passively along with the fluid flow, but exhibit a rotational motion governed by:

$$\left.\begin{aligned} \omega_{x'} &= \Omega_{x'} - S_{y'z'}\frac{\lambda^2-1}{\lambda^2+1}, \\ \omega_{y'} &= \Omega_{y'} + S_{x'z'}\frac{\lambda^2-1}{\lambda^2+1}, \\ \omega_{z'} &= \Omega_{z'}, \end{aligned}\right\} \tag{2.2}$$

obtained by equating the Jeffery torques (Jeffery 1922) to zero. Here, $\boldsymbol{\omega}$ denotes the particle rotation vector in the particle frame of reference $\langle x', y', z'\rangle$ with the origin at the centre of mass and z' aligned with the spheroid's axis of symmetry. For the special case of a sphere, i.e. $\lambda = 1$, the effect of the fluid strain-rate tensor $S_{i'j'}$ vanishes and the particle rotates along with the fluid rotation vector $\boldsymbol{\Omega}$. The particles were smaller than the Kolmogorov length scale so that the point-particle approach

can be justified. The one-way coupled simulation, neglecting flow field modulations and particle–particle collisions, can be justified for sufficiently dilute suspensions. The Jeffery torques, from which equation (2.2) was derived, have also been used to simulate the rotational behaviour of inertial spheroids by Zhang *et al.* (2001), Mortensen *et al.* (2008) and Challabotla, Zhao & Andersson (2015*a*).

Particle swarms, each consisting of 2.5 million spheroidal particles, with 10 different aspect ratios λ, were randomly distributed in the already fully developed turbulent Couette–Poiseuille flow field described by Yang *et al.* (2017*b*). The parameter space spans from flat disk-like particles (oblate spheroids with $\lambda = 0.01$) to long rod-like particles (prolate spheroids with $\lambda = 50$). The tendency of particles to concentrate preferentially in a turbulent flow field is an important phenomenon. Preferential segregation and concentration of spherical particles in the Couette–Poiseuille flow were investigated by Yang, Zhao & Andersson (2017*a*, 2018). These fascinating effects are caused by inertia and do not occur for inertia-free particles. It should therefore be emphasized that the present non-inertial spheroids remain randomly distributed over the entire flow field.

3. Results and discussion

3.1. *Preferential particle orientation in the laboratory frame*

Figure 2 shows the direction cosines of the particle orientation vector $\boldsymbol{p}$ relative to the axes $\langle x, y, z\rangle$ of the inertial coordinate frame in which the flow field is computed. Close to the stationary wall, tracer spheroids orient similarly as in the channel flow (Challabotla *et al.* 2015*b*). Long rods and thin disks align preferentially in the streamwise direction ($\langle|\cos\theta_x|\rangle \approx 0.8$) and the wall-normal direction ($\langle|\cos\theta_z|\rangle \approx 0.9$), respectively. Near the moving wall, where the mean shear is approaching zero, we observe that the disks orient similarly ($\langle|\cos\theta_z|\rangle \approx 0.9$) as they do close to the stationary wall, whereas the alignment of rods is relatively more random in the (x, y)-plane ($\langle|\cos\theta_x|\rangle \approx \langle|\cos\theta_y|\rangle \approx 0.6$) for $\lambda = 50$.

Even though the mean shear rate $\mathrm{d}U/\mathrm{d}z$ is finite and approximately $1/3$ of the magnitude of the vorticity fluctuations in the central region of the Couette–Poiseuille flow (Yang *et al.* 2017*b*), the spheroids tend towards almost random orientation irrespective of their aspect ratio λ. Randomized orientations of inertia-free spheroids were earlier observed in the shear-free centre of a plane channel flow by Challabotla *et al.* (2015*b*) and in HIT by Parsa *et al.* (2012), in both of which the vorticity field is (almost) isotropic.

According to figure 2(*a–c*), the preferential orientation of the spheroids is distinctly different near the two walls, whereas the orientation is almost isotropic in the centre region. A measure of the anisotropy of the orientation is shown in figure 2(*d*) where the particle orientation anisotropy POA is an indicator of the degree of departure from a random distribution $\langle|\cos\theta_i|\rangle = 0.5$, $i = 1, 2, 3$. Disk-like particles exhibit almost the same degree of anisotropy at both sides of the Couette–Poiseuille flow, whereas long rods orient more anisotropically near the stationary wall than in the vicinity of the moving wall. Earlier studies in HIT (Marcus *et al.* 2014; Ni *et al.* 2015) and WT (Zhao *et al.* 2015) show that the orientation of spheroids relative to the local fluid vorticity plays a vital role in particle rotational behaviour. It is therefore interesting to further examine how spheroids rotate with the different orientation distributions in the current Couette–Poiseuille flow.

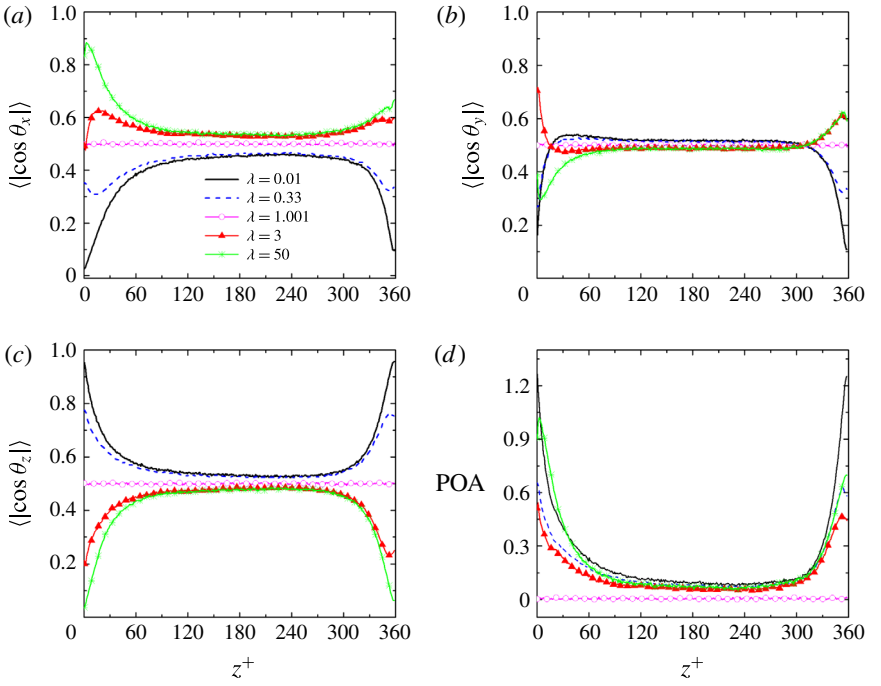

FIGURE 2. (Colour online) Mean direction cosines of particle orientation (*a*) $\langle|\cos\theta_x|\rangle$, (*b*) $\langle|\cos\theta_y|\rangle$ and (*c*) $\langle|\cos\theta_z|\rangle$ in streamwise, spanwise and wall-normal directions, respectively; (*d*) scalar measure of particle orientation anisotropy $\mathrm{POA} = |\langle|\cos\theta_x|\rangle - 0.5| + |\langle|\cos\theta_y|\rangle - 0.5| + |\langle|\cos\theta_z|\rangle - 0.5|$.

3.2. *Rotation modes in the particle frame*

We firstly explore how a spheroid rotates in the centre of the Couette–Poiseuille flow where the particles orient almost randomly (see figure 2), although the local fluid vorticity is anisotropic due to the presence of mean shear. Figure 3 shows the tumbling and spinning rates in the centre compared with earlier channel-flow results and experimental measurements in HIT. The close agreement indicates that the spheroids rotate in Mode I also in the present case, similarly to HIT and channel flow. Accordingly, we conclude that the isotropy of the particle orientation plays a more important role in the particle rotation mode, namely that rods spin and disks tumble, as long as their orientation is (almost) isotropic and no matter whether the vorticity field is isotropic (as in a channel centre and HIT) or anisotropic (as in the present flow). The slightly faster tumbling of disks and spinning of rods is most likely caused by the different Taylor-scale Reynolds number ($Re_\lambda \approx 52$ compared to $Re_\lambda \approx 24.8$ in the channel flow). Although a mean shear persists all across the Couette–Poiseuille flow, the shear rate $\mathrm{d}U/\mathrm{d}z$ in the centre region is only approximately 1.5 % of the shear rate at the stationary wall and is therefore approximately of the same order of magnitude as the vorticity fluctuations.

Zhao *et al.* (2015) showed that strong mean shear does play an important role in the particle rotation in the wall region where the particles are preferentially aligned relative to the channel walls. Let us therefore take a closer look at how the particles rotate in the Couette–Poiseuille flow where the mean shear is distinctly different at the two walls. Figures 4(*a*,*c*,*e*) and 4(*b*,*d*,*f*) show contours of tumbling and spinning

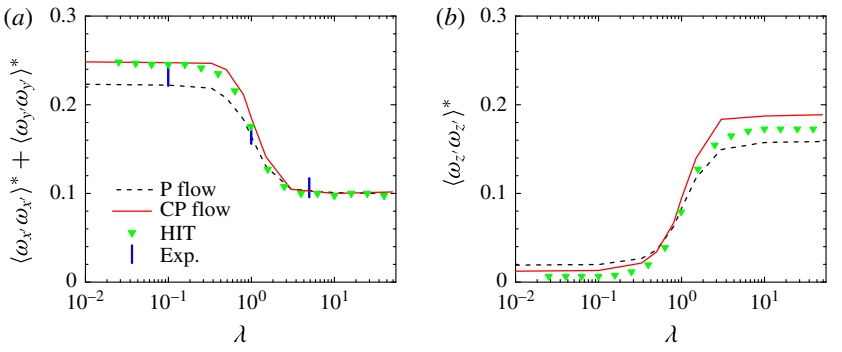

FIGURE 3. (Colour online) Channel-centre results of (*a*) tumbling component, and (*b*) spinning component of the particle rotation vector $\boldsymbol{\omega}$. Dashed black line: channel (P) flow (Zhao *et al.* 2015); solid red line: Couette–Poiseuille flow; green symbols: HIT (Byron *et al.* 2015); blue bars: experimental data (Parsa *et al.* 2012; Marcus *et al.* 2014). The superscript * indicates normalization by the local Kolmogorov time scale.

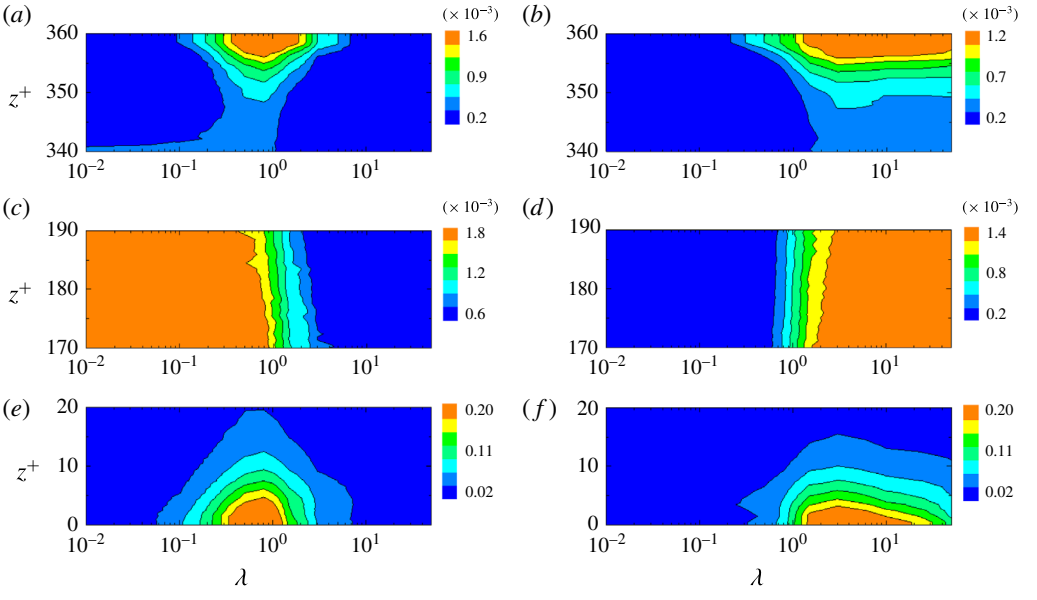

FIGURE 4. (Colour online) Contours of tumbling (*a*,*c*,*e*) and spinning (*b*,*d*,*f*) rates of spheroids near the moving wall, in the channel-centre region and near the stationary wall region (from top row to bottom row).

rates, respectively. The two plots in the middle row show that rods preferentially spin whereas disks preferentially tumble in the centre region. This Mode I rotation persists over a fairly wide core region and not only at the centre (i.e. at $z^+ = 180$, as shown in figure 3).

The particle rotation in the shear-dominated near-wall region from $z^+ = 0$ to 20 is shown in the lower row of figure 4. The highest tumbling rate is observed for spheroids with an aspect ratio slightly below unity ($\lambda \approx 0.8$), whereas the largest spinning rate is seen for intermediate aspect ratios $\lambda \approx 3$. Both spinning and tumbling

are suppressed with increasing asphericity. These findings are consistent with our earlier observations in channel-flow turbulence (Zhao *et al.* 2015). This is to be expected since the near-wall turbulence in the Couette–Poiseuille flow exhibits the same anisotropic vorticity field and the same coherent flow structures as the channel flow (see Yang *et al.* 2017*b*). While Zhao *et al.* (2015) showed results only at $z^+ = 10$, the present results reveal that the strong tumbling rate of slightly flattened disks ($\lambda \approx 0.8$) and the fast spinning rate of intermediate ($\lambda \approx 3$) rods decay rapidly with the distance from the stationary wall. This is likely to be associated with the decreasing mean shear rate $\mathrm{d}U/\mathrm{d}z$.

In contrast to the strong shear near the stationary wall, the shear rate is negligibly small near the moving wall. Here, we recall from figure 2 that disks preferentially aligned in the wall-normal direction whereas rods oriented almost randomly in the homogeneous (x, y)-plane. Since disk-like particles orient similarly near the moving and stationary walls, it is interesting to observe that disks also rotate similarly near the moving wall (figure 4 top row) as near the stationary wall (lower row). This is perhaps surprising since the local flow conditions are quantitatively and qualitatively different at the two walls of the Couette–Poiseuille flow. The mean shear rate, in particular, has its maximum at the stationary wall and almost vanishes at the moving wall.

On the other hand, the rotational behaviour of rod-like particles is different at the two walls. Short rods in the vicinity of the moving wall (figure 4 top row) almost equally spin and tumble. However, the tumbling rate decreases as the rods become longer, similarly to the centre region and at the stationary wall. The rapid spinning of the rods nevertheless persists even for the largest aspect ratio $\lambda = 50$ considered. This observation is in contrast to the gradual reduction of the spinning of long rods (increasing λ) near the stationary wall. Rod-like spheroids near the moving wall seem to exhibit Mode I rotation rather than Mode II rotation seen near the stationary wall as well as in channel-flow turbulence. The almost random orientation of rod-like particles in wall-parallel planes observed in figure 2 appears to play a dominating role in their rotational behaviour even in the moving wall region. This explains why the rods rotate differently at the two sides of the Couette–Poiseuille flow, while disk-like particles exhibit the same rotational behaviour in spite of the distinctly different mean shear rates. Here, we have learned that the preferential particle orientations have a deciding effect on the preferred mode of rotation. We recently demonstrated that the actual orientations of spheroidal particles are caused by alignment of rods (disks) with the strongest Lagrangian stretching (compression) direction in channel-flow turbulence and, furthermore, we conjectured this preferential alignment to be a universal phenomenon (Zhao & Andersson 2016).

The alignment of a non-spherical tracer particle relative to the local fluid vorticity has been used to explain the shape-dependent rotational behaviour (Gustavsson *et al.* 2014; Zhao *et al.* 2015). In figure 5 we examine the angle α between particle orientation $\boldsymbol{p}$ and fluid vorticity vector $2\boldsymbol{\Omega}$. Firstly, we observe that rods align in the direction of the vorticity vector in the centre region whereas disks orient normal to $\boldsymbol{\Omega}$. This preferred alignment causes rods to preferentially spin and disks to tumble (Ni *et al.* 2014; Zhao *et al.* 2015). In the region next to the stationary wall, the alignment of the tracer spheroids closely resembles the near-wall orientation in channel-flow turbulence (Zhao *et al.* 2015). In spite of the absence of mean shear, however, disk-like particles also align similarly near the moving wall. This observation explains the close similarity of disk rotation at the two distinctly different walls of the Couette–Poiseuille flow seen in figure 4. In contrast, however, rod-like particles orient themselves fundamentally differently relative to the local fluid vorticity near

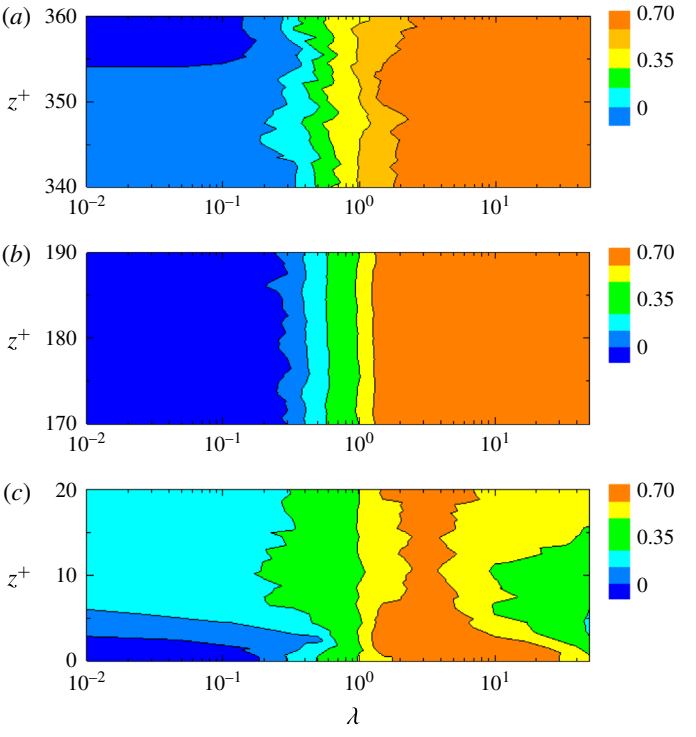

FIGURE 5. (Colour online) Cosine of the angle α between particle orientation vector $\boldsymbol{p}$ and fluid vorticity vector $2\boldsymbol{\Omega}$ near (*a*) the moving wall, (*b*) channel centre and (*c*) the stationary wall.

the two walls. Indeed, the alignment angle α of rods relative to $\boldsymbol{\Omega}$ in figure 5(*a*) is strikingly similar to the alignment in the centre region in figure 5(*b*). Yang *et al.* (2017*b*) showed that $\boldsymbol{\Omega}$ approaches a 2-D isotropy at the moving wall, see also figure 4(*b*). Now we have seen that this induces an orientational isotropy in wall-parallel planes of rod-like particles. This, in turn, might explain why the rotation of rods near the shear-free moving wall tends to Mode I.

In spite of the fact that the mean shear rate $\mathrm{d}U/\mathrm{d}z$ at the moving wall is lower than 1 % of the shear rate at the stationary wall, the disk-like particles orient and rotate similarly as they do near the stationary wall where conventional wall turbulence prevails in presence of a high shear rate. This suggests that even a very modest shear rate might play a non-negligible role provided that the particles are preferentially aligned in the flow field.

3.3. *Alignment with Lagrangian fluid stretching and compression*

The important role played by the orientation of differently shaped spheroids in their rotational behaviour in the Couette–Poiseuille flow, as demonstrated in § 3.2, raises the fundamental question regarding why spheroids orient differently relative to the local fluid vorticity near the moving and the fixed walls. According to the recent study by Ni *et al.* (2014), Lagrangian fluid stretching and compression cause preferential alignment of tracer spheroids in homogeneous isotropic turbulence (HIT), whereas Zhao & Andersson (2016) demonstrated that similar preferential alignments also exist

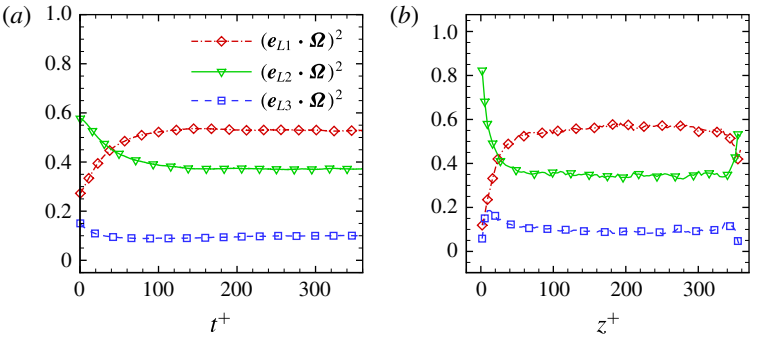

FIGURE 6. (Colour online) Alignment of the local fluid rotation vector $\boldsymbol{\Omega}$ relative to the three eigenvectors $\boldsymbol{e}_{Li}$ of the left Cauchy–Green strain tensor. Here, $\boldsymbol{e}_{L1}$ and $\boldsymbol{e}_{L3}$ are the maximum (extensional) and minimum (compressional) eigenvectors, respectively. (*a*) Time evolution of $\langle(\boldsymbol{e}_{Li}\cdot\boldsymbol{\Omega})^2\rangle$; (*b*) variation of $\langle(\boldsymbol{e}_{Li}\cdot\boldsymbol{\Omega})^2\rangle$ from the stationary wall at $z^+=0$ to the moving wall at $z^+=360$ sampled over an almost statistically steady state period from 300 to 360 ν/u_τ^2. Notice that the vorticity vector is two times the rotation vector, i.e. $2\boldsymbol{\Omega}$, and random alignment gives $\langle(\boldsymbol{e}_{Li}\cdot\boldsymbol{\Omega})^2\rangle=1/3$.

in anisotropic wall turbulence (WT). In both HIT and WT, long rods and thin disks were found to orient in the direction of Lagrangian fluid stretching and compression, respectively. Zhao & Andersson (2016) accordingly suggested that this is a universal mechanism. If so, the preferential alignment of tracer spheroids near the moving wall, as already observed in figure 5, can also be explained by means of Lagrangian fluid stretching. This as yet unanswered question will be addressed in the present subsection.

The Lagrangian stretching and compression directions are given by the maximum and minimum eigenvectors, $\boldsymbol{e}_{L1}$ and $\boldsymbol{e}_{L3}$, of the left Cauchy–Green strain tensor, respectively. We computed the Cauchy–Green strain tensor by using 50 000 stored Lagrangian trajectories together with the particle orientation vector $\boldsymbol{p}$, the particle rotation vector $\boldsymbol{\omega}$ and local fluid velocity gradient tensor A_{ij} for each of the particle shapes $\lambda=0.01$, 0.1, 0.33, 3, 10 and 50. When the simulation had been advanced for a time $324\nu/u_\tau^2$ after the tracer spheroids were initially introduced at randomly distributed locations, data were sampled and stored every $\Delta T=0.72\nu/u_\tau^2$ over a total time window $T=360\nu/u_\tau^2$, i.e. 500 fields. This sampling frequency is the same as that used by Zhao & Andersson (2016) in their channel-flow simulation, but the time window over which statistics were gathered was more than twice as long in the present study. The detailed procedure to compute the three eigenvectors of the Cauchy–Green strain tensor followed the same approach as in the earlier work by Parsa *et al.* (2011), Ni *et al.* (2014) and Zhao & Andersson (2016).

Firstly, we examine the correlation between fluid rotation and the three eigenvectors of the left Cauchy–Green tensor. We observe from figure 6(*a*) that a statistically steady state has been reached after approximately 150 viscous time units ν/u_τ^2. A modest alignment between the fluid rotation vector $\boldsymbol{\Omega}$ and the maximum eigenvector of the left Cauchy–Green strain tensor $\boldsymbol{e}_{L1}$ can be seen since $\langle(\boldsymbol{e}_{L1}\cdot\boldsymbol{\Omega})^2\rangle\approx0.53$. This alignment is in between the alignment $\approx$0.60 in HIT (Ni *et al.* 2014) and $\approx$0.50 at the centre of a turbulent channel flow (Zhao & Andersson 2016). The weaker alignment observed in the channel flow was ascribed to the alteration of the alignment of the fluid rotation vector $\boldsymbol{\Omega}$ with the eigenvector $\boldsymbol{e}_{L1}$ from the channel

walls to the channel centre. The fluid rotation vector was preferentially aligned in the direction of Lagrangian stretching only in the centre region of the channel, whereas the fluid rotation turned out to be perpendicular to both Lagrangian stretching and compression directions near the channel walls. In the Couette–Poiseuille flow, we observe in figure 6(*b*) similar alignments near the stationary wall and in the core region ($z^+ \approx 180$) as in turbulent channel flow. In spite of the finite mean shear rate $\mathrm{d}U/\mathrm{d}z$ over a wide core region in the Couette–Poiseuille flow, the same alignment $\langle(\boldsymbol{e}_{L1} \cdot \boldsymbol{\Omega})^2\rangle \approx 0.57$ as at the centre of the channel flow where $\mathrm{d}U/\mathrm{d}z = 0$ is found. This is remarkably close to the distinct alignment $\approx$0.60 in HIT.

However, near the moving wall, where the mean shear is almost zero, the fluid rotation vector still tends to align in the direction of Lagrangian fluid stretching, similarly to the channel-centre region and in HIT, but the preferential alignment is somewhat reduced to $\langle(\boldsymbol{e}_{L1} \cdot \boldsymbol{\Omega})^2\rangle \approx 0.40$ in the immediate vicinity of the wall, but yet significantly higher than 1/3 for random alignment. The observed similarities between the preferential orientations at the moving wall and in the centre region suggest that mean shear plays a crucial role in how the fluid vorticity orients relative to the Lagrangian fluid stretching direction. In turn, as already discussed in § 3.2, the relative alignment between particle orientation and fluid vorticity affects the particle's rotational mode.

As a final task we explore how tracer spheroids orient with the eigenvectors of the Cauchy–Green tensor. Results for six representative aspect ratios, from flat disks ($\lambda = 0.01$) to long rods ($\lambda = 50$), are shown in figures 7 and 8. The time evolution of the alignments in the Couette–Poiseuille flow in figure 7 are strikingly similar to the corresponding results in HIT and channel-flow turbulence reported by Ni *et al.* (2014) and Zhao & Andersson (2016), respectively. The rods preferentially orient in the direction of Lagrangian stretching $\boldsymbol{e}_{L1}$, while disks tend to align in the direction of Lagrangian compression $\boldsymbol{e}_{L3}$. It is noteworthy that the longest time it takes to reach a statistically steady state is for the most aspherical particles.

Of major interest is the alteration of the alignments across the Couette–Poiseuille flow, and in particular how the spheroids align themselves near the moving wall. The variation of $\langle(\boldsymbol{e}_{Li} \cdot \boldsymbol{p})^2\rangle$ with z has been sampled from $t^+ = 300$ to 360 and is presented in figure 8. Recall from figure 7 that almost all the adaption of the correlations $\langle(\boldsymbol{e}_{Li} \cdot \boldsymbol{p})^2\rangle$ to steady state has occurred at $t^+ = 300$. Unlike the distinctly asymmetric variation of the alignment of the fluid rotation $\boldsymbol{\Omega}$ relative to the eigenvectors $\boldsymbol{e}_{Li}$ in figure 6(*b*), the variations of $\langle(\boldsymbol{e}_{Li} \cdot \boldsymbol{p})^2\rangle$ from the stationary wall to the moving wall are surprisingly symmetric, irrespective of particle shape. The results near the stationary wall, e.g. $z^+ < 100$, are almost identical with the near-wall results in the channel flow (Zhao & Andersson 2016) and show a modest weakening of the preferential alignments close to the wall. In spite of the almost vanishing mean shear rate in the vicinity of the moving wall, the preferred alignments remain nearly the same as next to the stationary wall; i.e. rods align preferentially in the Lagrangian stretching direction and disks orient in the Lagrangian compression direction. The results in figure 8 suggest that the alignment of a particle's symmetry axis relative to the Lagrangian stretching (rod-like spheroids) or compression direction (disk-like spheroids) persists all across the Couette–Poiseuille flow, even though the flow structures and the vorticity field are strongly location dependent. These findings give further support to our conjecture that the preferential particle orientation in Lagrangian stretching or compression directions is robust and universal in both isotropic and anisotropic turbulence fields.

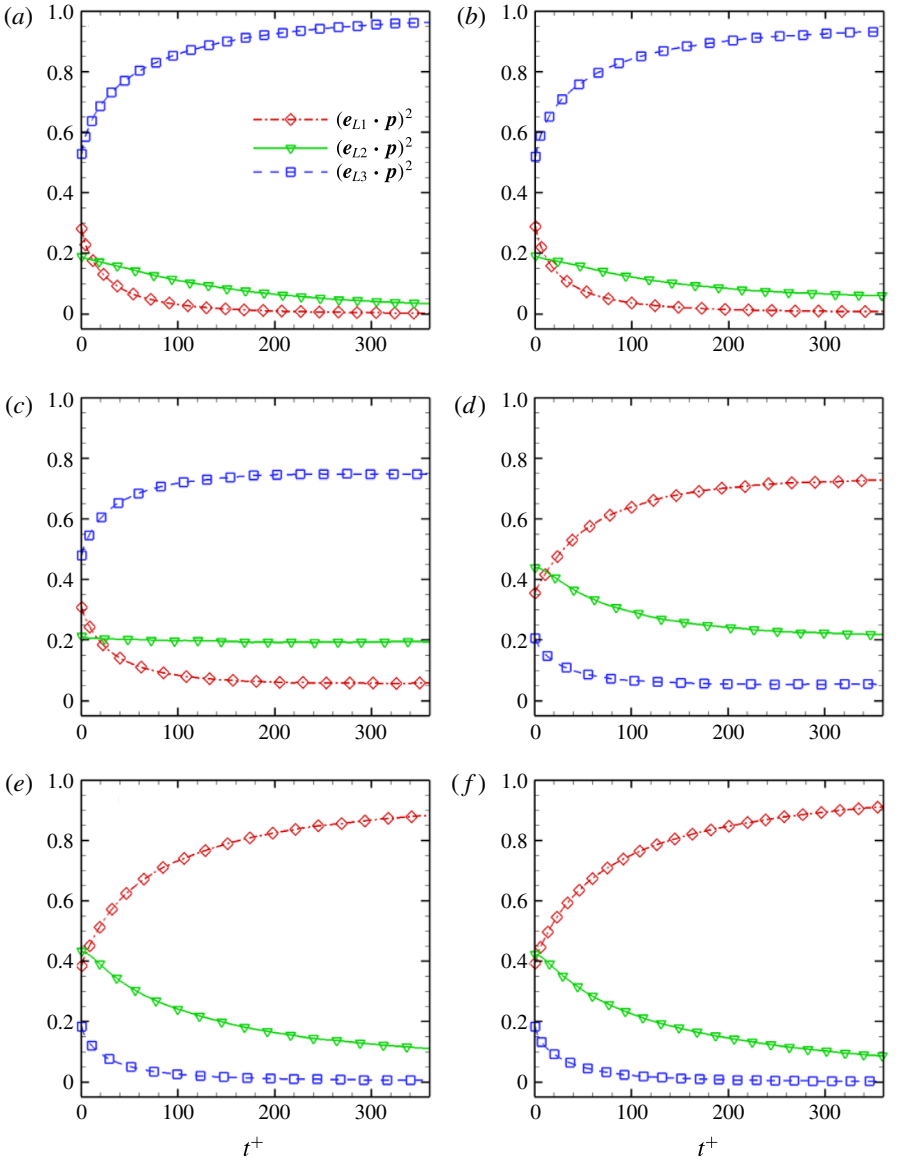

FIGURE 7. (Colour online) Time evolution of the alignment of the orientation vector $\boldsymbol{p}$ of spheroids with aspect ratio λ relative to the three eigenvectors $\boldsymbol{e}_{Li}$ of the left Cauchy–Green strain tensor. Here, $\boldsymbol{e}_{L1}$ and $\boldsymbol{e}_{L3}$ are the maximum (extensional) and minimum (compressional) eigenvectors, respectively. Random alignment gives $\langle(\boldsymbol{e}_{Li}\cdot\boldsymbol{p})^2\rangle = 1/3$. (*a*) $\lambda = 0.01$; (*b*) $\lambda = 0.1$; (*c*) $\lambda = 0.33$; (*d*) $\lambda = 3$; (*e*) $\lambda = 10$; (*f*) $\lambda = 50$.

On the other hand, the alignment of fluid vorticity $2\boldsymbol{\Omega}$ relative to the Lagrangian stretching direction $\boldsymbol{e}_{L1}$ is affected by the wall conditions. This leads to distinctly different alignments at the moving and stationary walls of the Couette–Poiseuille flow. It is already known that a particle's rotational behaviour is determined by how the particle orientates relative to the fluid vorticity, e.g. rods spin if aligned in the direction

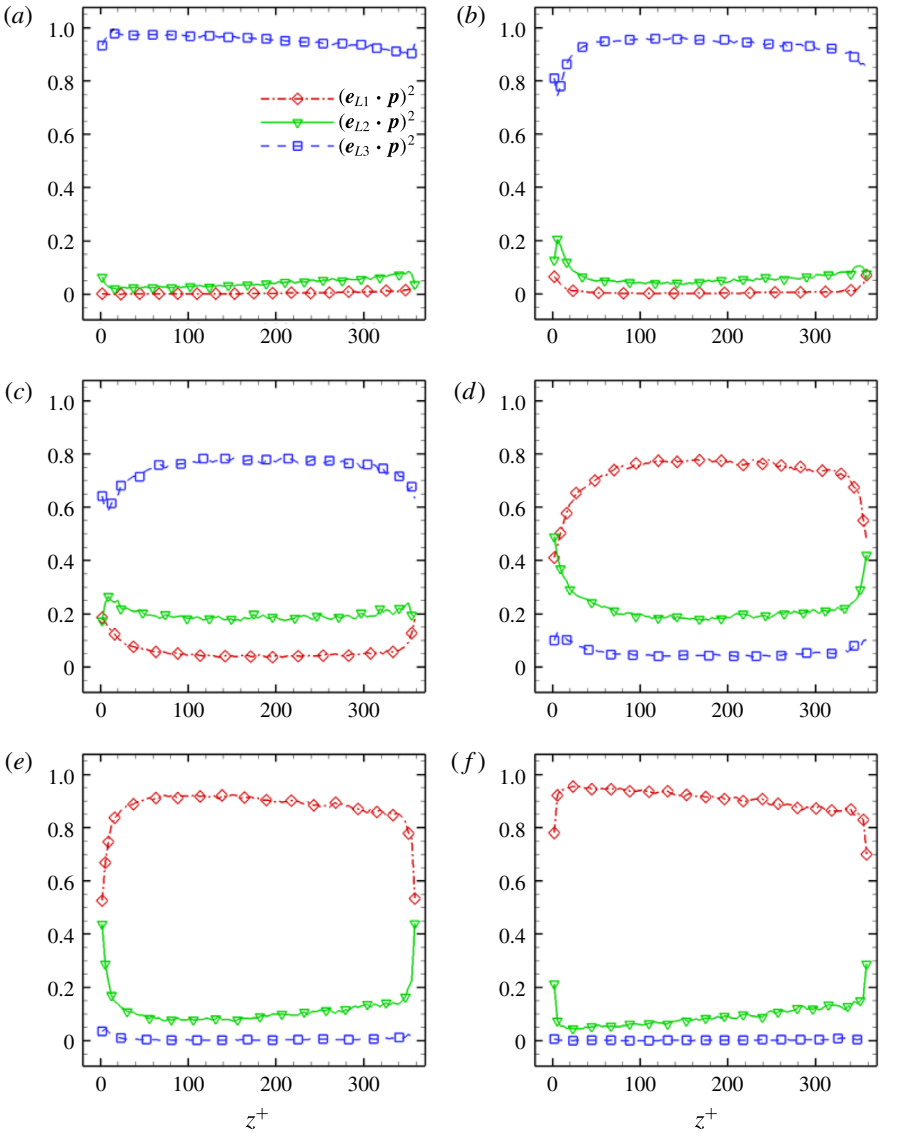

FIGURE 8. (Colour online) Variation of the alignment of the orientation vector $\boldsymbol{p}$ of spheroids with aspect ratio λ relative to the three eigenvectors $\boldsymbol{e}_{Li}$ of the left Cauchy–Green strain tensor from the stationary wall ($z^+ = 0$) to the moving wall ($z^+ = 360$). Here, $\boldsymbol{e}_{L1}$ and $\boldsymbol{e}_{L3}$ are the maximum (extensional) and minimum (compressional) eigenvectors, respectively. Random alignment gives $\langle(\boldsymbol{e}_{Li}\cdot\boldsymbol{p})^2\rangle = 1/3$. (*a*) $\lambda = 0.01$; (*b*) $\lambda = 0.1$; (*c*) $\lambda = 0.33$; (*d*) $\lambda = 3$; (*e*) $\lambda = 10$; (*f*) $\lambda = 50$.

of the fluid vorticity but tumble if orientated perpendicular to the fluid vorticity. Now, on the basis of the present analysis of how the fluid rotation vector and the particle orientation vector orient relative to Lagrangian stretching or compression directions, a more comprehensive explanation of earlier findings is provided and a more complete interpretation of tracer particles rotation modes in different flow fields has been given.

4. Concluding remarks

Rotational motion of spheroidal particles suspended in fluid turbulence is of vital importance for particle transport in general and collision outcome of nearby particles in particular. In this work, two distinctly different rotation modes of tracer spheroids reported in channel-flow turbulence (Zhao *et al.* 2015) were further investigated in a tailor-made Couette–Poiseuille flow. Contrary to the channel flow, the present flow case comprised a strongly sheared wall region (close to the stationary wall), a nearly homogeneous shear region (in the centre) and a region with almost negligible mean shear close to the moving wall. The objective was to achieve a better understanding of spheroidal particle rotation in sheared turbulence by exploring the different mechanisms that distinguish between the two rotation modes, namely the anisotropy of the particle orientation and fluid shear. These are considered to be the two major factors influencing the particle rotational behaviour.

In accordance with the present findings, particle orientation generally plays the most dominating role. In the centre region, the mean shear has practically no influence on particle rotation due to the isotropy of the particle orientations. In the two wall regions, however, mean shear plays a role in particle rotation whenever the particles are preferentially oriented (e.g. preferential alignments of disks and rods near the stationary wall in wall-normal and streamwise directions, respectively, and of disk-like particles in the wall-normal direction near the moving wall). The magnitude of the mean shear rate turned out to be of little importance for the particle rotation since disk-like particles were found to rotate in Mode II near the moving wall where the shear is rather modest (Yang *et al.* 2017*b*). As the isotropy of the orientation of rod-like particles increased near the moving wall, the effect of mean shear was weakened and rods rotated in Mode I, similarly to the centre region.

Furthermore, we measured the angle between the particle orientation vector and the local fluid vorticity vector. Similar particle alignments relative to fluid vorticity in the channel flow were observed in the centre region and near the stationary wall. Near the moving wall, however, long rods aligned with the direction of the vorticity vector and therefore spin preferentially. Thin disks, on the other hand, preferentially orientated perpendicular to the vorticity vector. Nevertheless, no preference of tumbling could be observed. This is due to the preferential orientation of disks in the wall-normal direction along with the influence of weak mean shear.

We finally examined if and how the differently shaped spheroids preferentially aligned with the direction of Lagrangian stretching and compression. The correlations between the orientation vector $\boldsymbol{p}$ and the left Cauchy–Green strain tensor $\boldsymbol{e}_{Li}$ explained the distinctly different alignments of the spheroids in the centre of the Couette–Poiseuille flow and near the two differently sheared walls. We were led to the conclusion that the preferential particle orientation along the Lagrangian stretching or compression directions is universally found in both isotropic and anisotropic turbulence and is independent of the mean shear rate.

In the present Couette–Poiseuille flow with vanishing mean shear at the moving wall, we observed roll-cell-like large-scale structures (LSSs) similarly to a plane Couette flow (Yang *et al.* 2017*b*), but these LSSs were considerably weaker and less coherent than those observed in DNS of plane Couette flow, e.g. Papavassiliou & Hanratty (1997) and Andersson, Lygren & Kristoffersen (1998). Such LSSs do have an impact on the distribution of inertial spheres in plane Couette flow (Bernardini, Pirozzoli & Orlandi 2013 and Richter & Sullivan 2013), but also in Couette–Poiseuille flow (Yang *et al.* 2017*a*, 2018). The non-spherical particles studied in the present paper have zero inertia and accordingly distribute themselves randomly across the

entire flow field. The orientations and rotations of these sub-Kolmogorov-sized particles are determined only by the local flow conditions, i.e. the small-scale eddies, whereas the size of the LSSs is of the order of the channel height $2h$, i.e. order-of-magnitudes larger than the particle size. The presence of LSSs does therefore not impact on the tiny inertialess spheroids studied in the present work.

The preferential orientations of spheroidal particles reported herein are based on the assumption that the spheroids are inertialess. This assumption offers two major advantages. Firstly, the interpretations of the results are freed from a discussion of preferential concentration and turbophoresis since tracer particles remain evenly distributed in the flow field and passively follow the fluid motion. Secondly, the analysis of correlations between the particle orientation and the eigenvectors of the left Cauchy–Green tensor in § 3.3 relies on the fact that tracer spheroids follow the same trajectories as the Lagrangian fluid trajectories.

Another flow in which effects of mean shear on particle orientation and rotation can be investigated is homogeneous shear turbulence (HST). Rogers & Moin (1987), Gerz, Schumann & Elghobashi (1989), Lee *et al.* (1990) and Schumacher & Eckhardt (2000) advocated different approaches towards DNS of HST, each with its own advantages and disadvantages (Sekimoto *et al.* 2016). A particularly attractive advantage of such flows over the Couette–Poiseuille flow is that the mean shear rate is the same everywhere. Potential direct or indirect interactions between the strongly sheared turbulence near the stationary wall and the weakly sheared region next to the moving wall are therefore excluded. However, the anisotropies of the fluctuating velocity and vorticity fields in HST are qualitatively different from the anisotropies observed in the vicinity of the moving wall in the Couette–Poiseuille flow (Yang *et al.* 2017*b*). In the nearly homogeneously sheared centre region, however, the turbulence field resembles HST. We are therefore inclined to conjecture that the observed particle behaviour in the centre region of the Couette–Poiseuille flow resembles what one would observe at similar mean shear rates in HST. However, the turbulence in the vicinity of the moving wall in the present Couette–Poiseuille flow is fundamentally different from HST. A primary motivation for the investigation was to explore particle behaviours in a flow field in which the role of the turbulence dominates over the effect of the mean shear rate. This objective cannot be fulfilled in HST.

The present findings of the roles played by preferential particle orientation and mean shear in rotation of non-spherical particles have obvious practical relevance, not only for plankton in the presence of wind shear, as mentioned in the introduction, but also for the behaviour of microplastics in marine environments (Barboza & Gimenez 2015).

Acknowledgements

The Research Council of Norway provided financial support through grant no. 250744 ‘Turbulence-plankton interactions’ and Sigma2 provided support of computational resources through grant no. NN2694K (Program for Supercomputing). The Second author was supported by Natural Science Foundation of China through grants nos 11702158, 91752205 and 11490551.

REFERENCES

ANDERSSON, H. I., LYGREN, M. & KRISTOFFERSEN, R. 1998 Roll cells in turbulent plane Couette flow: reality or artifact? In *Sixteenth International Conference on Numerical Methods in Fluid Dynamics* (ed. C. H. Bruneau), Lecture Notes in Physics, vol. 515, pp. 117–122. Springer.

ANDERSSON, H. I., ZHAO, L. & VARIANO, E. A. 2015 On the anisotropic vorticity in turbulent channel flows. *Trans. ASME J. Fluids Engng* **137** (8), 084503.

ARCEN, B., OUCHENE, R., KHALIJ, M. & TANIÉRE, A. 2017 Prolate spheroidal particles behavior in a vertical wall-bounded turbulent flow. *Phys. Fluids* **29** (3), 093301.

ARDEKANI, M. N., COSTA, P., BREUGEM, W. P., PICANO, F. & BRANDT, L. 2017 Drag reduction in turbulent channel flow laden with finite-size oblate spheroids. *J. Fluid Mech.* **816**, 43–70.

ARDESHIRI, H., BENKEDDAD, I., SCHMITT, F. G., SOUISSI, S., TOSCHI, F. & CALZAVARINI, E. 2016 Lagrangian model of copepod dynamics: clustering by escape jumps in turbulence. *Phys. Rev.* E **93**, 043117.

ARDESHIRI, H., SCHMITT, F. G., SOUISSI, S., TOSCHI, F. & CALZAVARINI, E. 2017 Copepods encounter rates from a model of escape jump behaviour in turbulence. *J. Plankton Res.* **39**, 878–890.

BALACHANDAR, S. 2009 A scaling analysis for point-particle approaches to turbulent multiphase flows. *Intl J. Multiphase Flow* **35**, 801–810.

BALACHANDAR, S. & EATON, J. K. 2010 Turbulent dispersed multiphase flow. *Annu. Rev. Fluid Mech.* **43**, 111–133.

BARBOZA, L. G. A. & GIMENEZ, B. C. G. 2015 Microplastics in the marine environment: current trends and future perspectives. *Marine Poll. Bull.* **97** (1), 5–12.

BARRY, M. T., RUSCONI, R., GUASTO, J. S. & STOCKER, R. 2015 Shear-induced orientational dynamics and spatial heterogeneity in suspensions of motile phytoplankton. *J. R. Soc. Interface* **12** (112), 20150791.

BECH, K. H., TILLMARK, N., ALFREDSSON, P. H. & ANDERSSON, H. I. 1995 An investigation of turbulent plane Couette flow at low Reynolds number. *J. Fluid Mech.* **286**, 291–325.

BERNARDINI, M., PIROZZOLI, S. & ORLANDI, P. 2013 The effect of large-scale turbulent structures on particle dispersion in wall-bounded flows. *Intl J. Multiphase Flow* **51**, 55–64.

BYRON, M., EINARSSON, J., GUSTAVSSON, K., VOTH, G. A., MEHLIG, B. & VARIANO, E. A. 2015 Shape-dependence of particle rotation in isotropic turbulence. *Phys. Fluids* **27** (3), 035101.

CHALLABOTLA, N. R., ZHAO, L. & ANDERSSON, H. I. 2015*a* Orientation and rotation of inertial disk particles in wall turbulence. *J. Fluid Mech.* **766**, R2.

CHALLABOTLA, N. R., ZHAO, L. & ANDERSSON, H. I. 2015*b* Shape effects on dynamics of inertia-free spheroids in wall turbulence. *Phys. Fluids* **27** (6), 061703.

COLEMAN, G. N., PIROZZOLI, S., QUADRIO, M. & SPALART, P. R. 2017 Direct numerical simulation and theory of a wall-bounded flow with zero skin friction. *Flow Turbul. Combust.* **99**, 553–564.

DO-QUANG, M., AMBERG, G., BRETHOUWER, G. & JOHANSSON, A. V. 2014 Simulation of finite-size fibers in turbulent channel flows. *Phys. Rev.* E **89**, 013006.

DURHAM, W. M., CLIMENT, E., BARRY, M., DE LILLO, F., BOFFETTA, G., CENCINI, M. & STOCKER, R. 2013 Turbulence drives microscale patches of motile phytoplankton. *Nature Comm.* **4**, 2148.

EATON, J. K. 2009 Two-way coupled turbulence simulations of gas-particle flows using point-particle tracking. *Intl J. Multiphase Flow* **35**, 792–800.

ESHGHINEJADFARD, A., HOSSEINI, S. A. & THEVENIN, D. 2017 Fully-resolved prolate spheroids in turbulent channel flows: a lattice Boltzmann study. *AIP Adv.* **7**, 095007.

GERZ, T., SCHUMANN, U. & ELGHOBASHI, S. E. 1989 Direct numerical simulation of stratified homogeneous turbulent shear flows. *J. Fluid Mech.* **200**, 563–594.

GOURLAY, T. 2006 Flow beneath a ship at small underkeel clearance. *J. Ship Res.* **50**, 250–258.

GUASTO, J. S., RUSCONI, R. & STOCKER, R. 2012 Fluid mechanics of planktonic microorganisms. *Annu. Rev. Fluid Mech.* **44**, 373–400.

GUSTAVSSON, K., EINARSSON, J. & MEHLIG, B. 2014 Tumbling of small axisymmetric particles in random and turbulent flows. *Phys. Rev. Lett.* **112** (1), 014501.

HANDLER, R. A., SWEAN, T. F., LEIGHTON, R. I. & SWEARINGEN, J. D. 1993 Length scales and the energy balance for turbulence near a free surface. *AIAA J.* **31**, 1998–2007.

JEFFERY, G. B. 1922 The motion of ellipsoidal particles immersed in a viscous fluid. *Proc. R. Soc. Lond.* A **102** (715), 161–179.

JEONG, J., HUSSAIN, F., SCHOPPA, W. & KIM, J. 1997 Coherent structures near the wall in a turbulent channel flow. *J. Fluid Mech.* **332**, 185–214.

JIMÉNEZ, J. 1997 Oceanic turbulence at millimeter scales. *Sci. Mar.* **61**, 47–56.

KATZ, J. 2006 Aerodynamics of race cars. *Annu. Rev. Fluid Mech.* **38**, 27–63.

KIM, J., MOIN, P. & MOSER, R. 1987 Turbulence statistics in fully developed channel flow at low Reynolds number. *J. Fluid Mech.* **177**, 133–166.

KURODA, A., KASAGI, N. & HIRATA, M. 1995 Direct numerical simulation of turbulent Couette-Poiseuille flows: effect of mean shear rate on the near wall turbulence structures. In *Turbulent Shear Flows* (ed. F. Durst, N. Kasagi, B. E. Launder, F. W. Schmidt, K. Suzuki & J. H. Whitelaw), vol. 9, pp. 241–257. Springer.

LEE, M. J., KIM, J. & MOIN, P. 1990 Structure of turbulence at high shear rate. *J. Fluid Mech.* **216**, 561–583.

LUCCI, F., FERRANTE, A. & ELGHOBASHI, S. 2010 Modulation of isotropic turbulence by particles of Taylor length-scale size. *J. Fluid Mech.* **650**, 5–55.

MARCUS, G. G., PARSA, S., KRAMEL, S., NI, R. & VOTH, G. A. 2014 Measurements of the solid-body rotation of anisotropic particles in 3D turbulence. *New J. Phys.* **16** (10), 102001.

MORTENSEN, P. H., ANDERSSON, H. I., GILLISSEN, J. J. J. & BOERSMA, B. J. 2008 Dynamics of prolate ellipsoidal particles in a turbulent channel flow. *Phys. Fluids* **20** (9), 093302.

NAGAOSA, R. & HANDLER, R. A. 2003 Statistical analysis of coherent vortices near a free surface in a fully developed turbulence. *Phys. Fluids* **15**, 375–394.

NI, R., KRAMEL, S., OUELLETTE, N. T. & VOTH, G. A. 2015 Measurements of the coupling between the tumbling of rods and the velocity gradient tensor in turbulence. *J. Fluid Mech.* **766**, 202–225.

NI, R., OUELLETTE, N. T. & VOTH, G. A. 2014 Alignment of vorticity and rods with Lagrangian fluid stretching in turbulence. *J. Fluid Mech.* **743**, R3.

OUCHENE, R., KHALIJ, M., ARCEN, B. & TANIÉRE, A. 2016 A new set of correlations of drag, lift and torque coefficients for non-spherical particles and large Reynolds number. *Powder Tech.* **303**, 33–43.

PAN, Y. & BANERJEE, S. 1995 A numerical study of free-surface turbulence in channel flow. *Phys. Fluids* **7**, 1649–1663.

PAPAVASSILIOU, D. V. & HANRATTY, T. J. 1997 Interpretation of large-scale structures observed in a turbulent plane Couette flow. *Intl J. Heat Fluid Flow* **18**, 55–69.

PARSA, S., CALZAVARINI, E., TOSCHI, F. & VOTH, G. A. 2012 Rotation rate of rods in turbulent fluid flow. *Phys. Rev. Lett.* **109**, 134501.

PARSA, S., GUASTO, J. S., KISHORE, M., OUELLETTE, N. T., GOLLUB, J. P. & VOTH, G. A. 2011 Rotation and alignment of rods in two-dimensional chaotic flow. *Phys. Fluids* **23**, 043302.

PEDLEY, T. J. & KESSLER, J. O. 1992 Hydrodynamic phenomena in suspensions of swimming microorganisms. *Annu. Rev. Fluid Mech.* **24**, 313–358.

PUMIR, A. & WILKINSON, M. 2011 Orientation statistics of small particles in turbulence. *New J. Phys.* **13**, 093030.

REIDENBACH, M. A., KOSEFF, J. R. & KOEHL, M. 2009 Hydrodynamic forces on larvae affect their settlement on coral reefs in turbulent, wave-driven flow. *Limnol. Oceanogr.* **54**, 318–330.

RICHTER, D. H. & SULLIVAN, P. P. 2013 Momentum transfer in a turbulent, particle-laden Couette flow. *Phys. Fluids* **25**, 053304.

ROBINSON, S. K. 1991 Coherent motions in the turbulent boundary layer. *Annu. Rev. Fluid Mech.* **23**, 601–639.

ROGERS, M. M. & MOIN, P. 1987 The structure of the vorticity field in homogeneous turbulent flows. *J. Fluid Mech.* **176**, 33–66.

ROSÉN, T., LUNDELL, F. & AIDUN, C. K. 2014 Effect of fluid inertia on the dynamics and scaling of neutrally buoyant particles in shear flow. *J. Fluid Mech.* **738**, 563–590.

RUIZ, J., MACÍAS, D. & PETERS, F. 2004 Turbulence increases the average settling velocity of phytoplankton cells. *Proc. Natl Acad. Sci. USA* **101**, 17720–17724.

SCHUMACHER, J. & ECKHARDT, B. 2000 On statistically stationary homogeneous shear turbulence. *Europhys. Lett.* **52**, 627–632.

SEKIMOTO, A., DONG, S. & JIMÉNEZ, J. 2016 Direct numerical simulation of statistically stationary and homogenous shear turbulence and its relation to other shear flows. *Phys. Fluids* **28**, 035105.

SIEWERT, C., KUNNEN, R. P. J., MEINKE, M. & SCHRÖDER, W. 2014 Orientation statistics and settling velocity of ellipsoids in decaying turbulence. *Atmos. Res.* **142**, 45–56.

SPENCER, N. B., LEE, L. L., PARTHASARATHY, R. N. & PAPAVASSILIOU, D. V. 2009 Turbulence structure for plane Poiseuille–Couette flow and implications for drag reduction over surfaces with slip. *Can. J. Chem. Engng* **87**, 38–46.

THURLOW, E. M. & KLEWICKI, J. C. 2000 Experimental study of turbulent Poiseuille–Couette flow. *Phys. Fluids* **12**, 865–875.

VOTH, G. A. & SOLDATI, A. 2017 Anisotropic particles in turbulence. *Annu. Rev. Fluid Mech.* **49**, 249–276.

YANG, K., ZHAO, L. & ANDERSSON, H. I. 2017*a* Preferential particle concentration in wall-bounded turbulence with zero skin friction. *Phys. Fluids* **29**, 113302.

YANG, K., ZHAO, L. & ANDERSSON, H. I. 2017*b* Turbulent Couette–Poiseuille flow with zero wall shear. *Intl J. Heat Fluid Flow* **63**, 14–27.

YANG, K., ZHAO, L. & ANDERSSON, H. I. 2018 Particle segregation in turbulent Couette–Poiseuille flow with vanishing wall shear. *Intl J. Multiphase Flow* **98**, 45–55.

ZHANG, H., AHMADI, G., FAN, F. G. & MCLAUGHLIN, J. B. 2001 Ellipsoidal particles transport and deposition in turbulent channel flows. *Intl J. Multiphase Flow* **27**, 971–1009.

ZHAO, L. & ANDERSSON, H. I. 2016 Why spheroids orient preferentially in near-wall turbulence. *J. Fluid Mech.* **807**, 221–234.

ZHAO, L., CHALLABOTLA, N. R., ANDERSSON, H. I. & VARIANO, E. A. 2015 Rotation of nonspherical particles in turbulent channel flow. *Phys. Rev. Lett.* **115**, 244501.